The Astrophysical Journal, 719:634–641, 2010 August 10 doi:10.1088/0004-637X/719/1/634

FIRST ORBITAL SOLUTION FOR THE NON-THERMAL EMITTER Cyg OB2 NO. 9*

Y. Nazé[1,6], Y. Damerdji[1], G. Rauw[1,6], D. C. Kiminki[2], L. Mahy[1], H. A. Kobulnicky[2], T. Morel[1], M. De Becker[1,3], P. Eenens[4], and C. Barbieri[5]
[1] GAPHE, Département AGO, Université de Liège, Allée du 6 Août 17, Bat. B5C, B4000-Liège, Belgium; naze@astro.ulg.ac.be
[2] Department of Physics & Astronomy, University of Wyoming, Laramie, WY 82070, USA
[3] Observatoire de Haute-Provence, F-04870 St. Michel l'Observatoire, France
[4] Departamento de Astronomia, Universidad de Guanajuato, Apartado 144, 36000 Guanajuato, GTO, Mexico
[5] Dipartimento di Astronomia, Universitá degli studi di Padova, vicolo Osservatorio 2, 35122 Padova, Italy
Received 2010 February 3; accepted 2010 June 14; published 2010 July 22

ABSTRACT

After the first detection of its binary nature, the spectroscopic monitoring of the non-thermal radio emitter Cyg OB2 No. 9 ($P = 2.4$ yr) has continued, doubling the number of available spectra of the star. Since the discovery paper of 2008, a second periastron passage has occurred in 2009 February. Using a variety of techniques, the radial velocities could be estimated and a first, preliminary orbital solution was derived from the He I λ5876 line. The mass ratio appears close to unity and the eccentricity is large, i.e., 0.7–0.75. X-ray data from 2004 and 2007 are also analyzed in quest of peculiarities linked to binarity. The observations reveal neither large overluminosity nor strong hardness, but it must be noted that the high-energy data were taken after the periastron passage, at a time where colliding wind emission may be low. Some unusual X-ray variability is however detected, with a 10% flux decrease between 2004 and 2007. To clarify their origin and find a more obvious signature of the wind–wind collision, additional data, taken at periastron and close to it, are needed.

Key words: binaries: spectroscopic – stars: early-type – stars: emission-line, Be – stars: individual (Cyg OB2 No. 9) – X-rays: stars

Online-only material: color figures

1. INTRODUCTION

As the objects mainly responsible for mechanical input, chemical enrichment, and ionizing radiation in galaxies, massive stars (i.e., with masses $>10\,M_{\odot}$) are important objects of the stellar population. However, these objects are rare: in the Galaxy, about 300 Wolf–Rayet stars (WRs; i.e., fewer than exoplanets; van der Hucht 2006), as well as about 400 O-type stars (plus 700 candidates that are sometimes classified as O; see Sota et al. 2008), are known. A natural consequence is that many aspects of these stars remain poorly known, even in the case of their major property, the stellar wind, for which "basic" quantities such as the mass-loss rates are still heavily debated at the present time (e.g., Sundqvist et al. 2010).

In this context, non-thermal radio emitters associated with massive stars form an even more limited group, with fewer than 40 cases known in our Galaxy (De Becker 2007; Benaglia 2010), but these objects can provide unique insights into the physics of stellar winds since both phenomena are intimately linked.

Observing such non-thermal radio emission implies two prerequisites: the presence of both a magnetic field and a population of relativistic electrons. Direct detection of the former is notoriously difficult in massive stars, which display only few broad lines and therefore have a weak Zeeman signature. However, as some of the descendants of massive stars (i.e., neutron stars) are clearly magnetic, there was little doubt that magnetic fields are not totally absent in these objects. Indeed, the last decade saw the collection of first evidence of magnetism in massive stars thanks to spectropolarimetric monitorings (e.g., Donati et al. 2002, with even a tentative detection in a non-thermal emitter in Hubrig et al. 2008).

The second requirement, the population of relativistic electrons, is ultimately linked to the presence of shocks in the ionized winds (for a review, see De Becker 2007). Acceleration then takes place through the first-order Fermi mechanism, also called "diffusive shock acceleration," where electrons iteratively gain energy by crossing the shock zone several times. Shocks are not ubiquitous in stellar winds: they can either be intrinsic to the winds themselves (as the line-driven mechanism producing the wind is intrinsically unstable) or arise in massive binaries from the collision of the two stellar winds. Recent theoretical modeling showed that only the latter can account for the observed non-thermal radio emission (van Loo et al. 2005). Indeed, the large majority of the known cases of non-thermal emitters are confirmed or suspected binaries—only 3 of the 17 WRs and 3 of the 16 O stars listed by De Becker (2007) totally lack evidence for binarity. However, this can often be explained by inadequate monitoring, or sometimes simply by the absence of any monitoring. Once an adequate observing campaign is organized, proofs of binarity are often found, as exemplified by our recent successes in this domain (e.g., Cyg OB2 No. 8A, De Becker et al. 2004; 9 Sgr, Rauw et al. 2005b; G. Rauw et al. 2011, in preparation), which greatly improved the multiplicity census of non-thermal radio emitters associated with O-type stars. Among the remaining objects without evidence of multiplicity, the early-type star Cyg OB2 No. 9 (O5I) is clearly a target of choice.

Located in the rich association Cyg OB2 (Knödlseder 2000), Cyg OB2 No. 9 was one of the first O stars shown to be a non-thermal radio emitter (Abbott et al. 1984). The presence of this emission remained problematic for years. The first direct evidence of the binary nature of Cyg OB2 No. 9 was only reported in 2008 thanks to a dedicated, long-term spectroscopic

* Based on observations collected at the Haute-Provence Observatory and with *XMM-Newton*, an ESA Science Mission with instruments and contributions directly funded by ESA Member States and the USA (NASA).
[6] Research Associate FRS-FNRS.

monitoring (Nazé et al. 2008). In the same year, van Loo et al. (2008) revealed a long-term modulation of the radio emission and derived for it a period of 2.355 yr, interpreted as being associated with the binary orbit. This radio flux appeared minimum when the stellar lines were unblended in the optical spectrum. Up to now, however, a full orbital solution and a detailed modeling of the system are still missing. This paper aims at beginning to fill this gap by tackling the first problem: the derivation of the orbital parameters.

It must be recalled that Cyg OB2 No. 9 is not an easy star to analyze. On the one hand, it is strongly extinguished ($E[B-V] = 2.11$; Massey & Thompson 1991) with two consequences. First, the spectrum of Cyg OB2 No. 9 displays very strong interstellar lines, often affecting the stellar lines, even those usually quite uncontaminated (e.g., C IV λ5812). Second, the star appears faint, especially at blue wavelengths where most lines used for spectral classification are found. On the other hand, the stellar lines remain totally blended for about 80% of the orbit; a clear doubling of the lines can only be seen during a few months of the 2.355 yr period. This is due to the large eccentricity of the system but also to the width of the lines ($\mathrm{FWHM}_{\mathrm{He\,I}\,\lambda5876} \sim 3$ Å).

Despite these difficulties, we have continued our monitoring of Cyg OB2 No. 9, with the hope of improving our knowledge of this system. This paper reports on the new data collected since 2008 January, including at orbital phases close to the periastron passage of 2009 (the periastron itself was unobservable as Cyg OB2 No. 9 was in conjunction with the Sun at that time). A preliminary orbital solution is presented here for the first time. This is a necessary and crucial step toward the full modeling of the system and the derivation of the winds' parameters.

Complementary high-energy data are also presented here, as they directly relate to the question of colliding winds. At first, one could expect for these peculiar objects a non-thermal X-ray emission, a direct companion to that observed in the radio range. However, direct and undisputed evidence of such emission is still lacking: its detection awaits the advent of sensitive observatories in the >10 keV range (De Becker et al. 2009). In the meantime, one could however try to find evidence for wind–wind collision in the *thermal* X-ray emission which dominates the 0.3–10 keV range, the preferred bandwidth of the current sensitive facilities (*XMM-Newton*, *Chandra*). Indeed, some binaries display strong wind–wind shocks which are able to produce very hot plasma, and hence hard and bright X-rays. Moreover, in these cases, the X-ray emission is modulated as the stars orbit each other (for a review, see Güdel & Nazé 2009). It is therefore important to check whether the X-ray emission of Cyg OB2 No. 9 bears the signature of wind–wind collision. This would yield a further proof of the link between binarity and non-thermal radio emission, as well as additional constraints on the winds' parameters.

The paper is organized as follows. Sections 2 and 3 present the optical data set and its analysis, Section 4 details the X-ray properties of Cyg OB2 No. 9, and Section 5 summarizes our results.

2. THE OPTICAL DATA SET

The observations obtained until early 2008 January have been described at length in Nazé et al. (2008), and only the new data will be described here. These new observations were obtained at the Haute-Provence Observatory (OHP; France) and the Wyoming Infrared Observatory (WIRO; USA); an archival data set taken at San Pedro Mártir (SPM, Mexico) in 2004 has been added to the new analysis. A journal of these observations is provided in Table 1.

Table 1
Journal of Observations

Instrument	Date	N	Δλ (Å)	R	S/N
Espresso	3288.806	1	3780–6950	18000	100
Aurélie	4560.563	3	5500–5900	8800	40
	4591.557	3	5500–5900	8800	80
	4620.472	3	5500–5900	8800	70
	4652.481	3	5500–5900	8800	70
	4680.444	4	5500–5900	8800	60
	4711.439	1	4450–4900	7000	30
	4715.388	3	5500–5900	8800	75
WIRO	4672.764	4	5300–6700	4000	200
	4746.743	1	5300–6700	4000	150
	4818.624	1	5300–6700	4000	220
	4842.070	2	5300–6700	4000	150
Sophie	4906.675	3	3900–6900	35000	65
	4936.968	3	3900–6900	35000	80
	4953.595	1	3900–6900	35000	75
	5006.497	2	3900–6900	35000	80
	5022.578	2	3900–6900	35000	80
	5058.433	1	3900–6900	35000	75
	5079.965	2	3900–6900	35000	70
	5123.370	1	3900–6900	35000	75
	5142.240	1	3900–6900	35000	95

Note. Heliocentric Julian Dates (mean values if $N \neq 1$) are given in the format HJD-2,450,000; N is the number of spectra taken; Δλ is the wavelength range; R is the resolving power ($\lambda/\mathrm{FWHM}_{\mathrm{calib}}$); and S/N is the average signal-to-noise ratio of the individual exposures around 5835 Å (or 4555 Å for the blue spectrum).

At the OHP, six additional spectra in the yellow range and one in the blue range were obtained in 2008 using the 1.52 m telescope equipped with the Aurélie spectrograph (grating 3, $R \sim 9000$). In 2009, the Sophie échelle instrument ($R = 35{,}000$, 39 orders over the domain 3900–6900 Å) installed on the 1.93 m telescope observed the system nine times in the high-efficiency mode. For each data set, the typical exposure time was 1800–7200 s; the observations were sometimes split into several individual exposures which were finally combined if taken within 1–15 days. The data were first reduced in a standard way, smoothed by a moving box average and finally normalized. Note that data from 2009 August 10 and 13 were unusable due to a technical problem.

In Wyoming, the observations were obtained with the 2.3 m telescope equipped with the WIRO-Longslit spectrograph (1800 l mm^{-1} grating in the first order, $R \sim 4000$). Exposure times varied from 720 to 5400 s (generally in multiples of 600–900 s) depending on weather conditions. All data sets were reduced using standard IRAF reduction routines as outlined in Kiminki et al. (2007).

One archival échelle spectrum, taken with the 2.1 m telescope of SPM equipped with the Espresso spectrograph ($R = 18{,}000$, 27 orders over the range 3780–6950 Å), was also made available and added to our data set. These data were reduced in a standard way using MIDAS.

To improve the wavelength calibration, we took advantage of the high reddening and used several narrow, well-marked diffuse interstellar bands (DIBs) close to major spectral lines. Their velocity shifts relative to a chosen reference data set (the échelle spectra taken by Sophie in 2007 October) were measured using a cross-correlation method. The measured radial velocities (RVs) of the stellar lines (see below) were then corrected by the

shifts derived from a close DIB (e.g., DIB λ5780 for He I λ5876). This ensures that the wavelength calibration is correct to within 5–10 km s^{-1} in the worst case.

In total, our data set now comprises 20 échelle spectra (Sophie at OHP, AFOSC at Asiago, and Espresso at SPM), 8 long-slit spectra at red wavelengths (Aurélie at OHP, Asiago), 10 yellow spectra (Aurélie at OHP), 1 blue spectrum (Aurélie at OHP), and 4 yellow-to-red, low-resolution spectra (WIRO). These data were taken between 2003 and 2009, with a more intense monitoring since 2006.

3. TOWARD A FIRST ORBITAL SOLUTION

3.1. Radial Velocities

To derive an orbital solution, it is necessary to (1) choose adequate stellar lines and (2) secure good estimates of the RVs.

Choosing reliable stellar lines is not an easy task for Cyg OB2 No. 9. With strong interstellar lines and low signal-to-noise ratios, many lines have to be discarded. While the splitting is seen near periastron for He I λ4471 and He II λ4542, the strong noise in the blue domain prevents us from deriving good RV estimates from these lines throughout the whole orbit. Metal lines, such as C IV λλ5801, 5812 or O III λ5592, are strongly contaminated by interstellar lines, rendering their measurement difficult. In addition, the two stars of the system appear so similar in spectral type that there is no obvious, sufficiently strong stellar line belonging to only one component of the pair. Also, the data do not always cover the same wavelength range and the chosen line should indeed belong to the most frequently recorded domain. Our best choice for RV determination is thus He I λ5876, which is simultaneously strong and free from interstellar contamination. However, there is a caveat to this choice: this line is sometimes polluted by emission in some extreme O-type stars. In our data set, there is no emission above the continuum level, but it is difficult to exclude with 100% confidence the presence of faint emission which would slightly "fill" the photospheric absorptions. Our results are thus clearly preliminary.

The stellar lines have first been fitted by Gaussians (usually one, with two only for the 2–3 clearly unblended spectra). The last column of Table 2 gives the result of a single Gaussian fit to the blended data (i.e., $0.1 < \phi < 0.9$). However, as the line splitting has clearly been detected (Nazé et al. 2008), at least during some part of the orbit, we tried to improve this RV determination by using the correlation method (TODCOR; see Zucker & Mazeh 1994), the disentangling method (González & Levato 2006; Mahy et al. 2010), and the χ^2-mapping method. Used on a sole line (He I λ5876), the first two methods give poor results. As TODCOR involves the convolution between a typical line shape (i.e., a Gaussian in our case) and the spectrum (reduced here to one single line), the peak of the cross-correlation function is broad, increasing the error bars on the RVs to unacceptable levels. Even at maximum separation, TODCOR does not always yield results within 10 km s^{-1} of the simple two-Gaussian fitting, and was thus discarded. Disentangling the He I line also proved unreliable, the main reason being that due to the orbital configuration, the lines are only partially separated when the primary is blueshifted and the secondary is redshifted. The reverse situation, redshifted primary and blueshifted secondary, is never observed (Figure 1, left). Therefore, the only solution for fitting two components in He I λ5876 was first to fit each component at maximum separations using Gaussians and then to shift these two Gaussians, keeping their shape (width and depth) constant, to find the minimum χ^2 for each spectrum (Figure 1, right). The RVs determined with this method are listed in the third and fourth columns of Table 2. When available and close to maximum separation, results from this method are similar for He II λ6683. Figure 2 shows the evolution of the RVs, the two periastron passages can be clearly seen, as well as the relative constancy of the RVs during most of the period. When the two components are blended, the RVs are still rather uncertain, as the separation is then much smaller than the line width.

We have detailed above the numerous caveats concerning our measurements and our data (blending during most of the orbit, possible slight contamination by emission, χ^2-mapping versus single Gaussian fit). Caution should thus apply, but it should also be stressed that these observations and measurements represent the best data set available for Cyg OB2 No. 9. Deriving an orbital solution using these RVs was thus attempted.

Table 2
RVs of the He I line at 5875.62 Å, with Heliocentric Julian Dates Given in the Format HJD-2,450,000

Date	ϕ_{SB2}	RV_1 (km s^{-1})	RV_2 (km s^{-1})	RV_{Gauss} (km s^{-1})
3288.806	0.12	−60.3	2.5	−41.4
3726.231	0.63	−52.6	15.9	−22.6
3887.493	0.82	−47	34	−7.0
3990.455	0.94	−78.1	70.2	
4022.252	0.98	−142.5	96.1	
4036.237	1.00	−119.9	130.9	
4051.389	0.02	−79.2	112.7	
4066.298	0.03	−108	19.6	
4244.476	0.24	−24.2	−4.9	−16.7
4303.495	0.31	−27.9	1	−21.3
4324.427	0.34	−36	−0.4	−19.6
4348.765	0.37	−26.6	−0.4	−17.3
4379.063	0.40	−25.9	−10.1	−17.1
4463.748	0.50	−22	1.8	−10.1
4472.247	0.51	−24.7	−1	−17.8
4560.563	0.61	−29.1	26.2	−18.1
4591.557	0.65	−18.8	23.8	8.0
4620.472	0.68	−23.9	23.6	14.2
4652.481	0.72	−21.8	19.8	−1.0
4672.764	0.75	−26.3	11.5	−2.7
4680.444	0.76	−22.4	29.8	13.0
4715.388	0.80	−11.4	23	1.3
4746.743	0.83	−17.5	24.2	0.7
4818.624	0.92	−30.8	52.4	
4842.070	0.95	−48.4	71.1	
4906.675	0.02	−97.1	64.5	
4936.968	0.06	−68.9	17.3	
4953.595	0.08	−54.7	7.5	
5006.497	0.14	−40.3	3.8	−24.3
5022.578	0.16	−36.5	−10.9	−25.9
5058.433	0.20	−27.4	−8.2	−15.9
5079.965	0.22	−32.7	−6.8	−17.2
5123.370	0.28	−26.3	−15.2	−20.0
5142.240	0.30	−28.2	−10.7	−19.1

Notes. The RVs have been corrected for remaining shifts using the DIB at 5780 Å (see the text). Phases correspond to the SB2 solution (second column of Table 3).

3.2. Orbital Solution

Single-lined spectroscopic binary (SB1) solutions were calculated in several steps. First, the best-fit period was selected using the Fourier method of Heck et al. (1985; see also remarks in Gosset et al. 2001). A polynomial fit of the folded RV curve was then calculated and an approached orbital solution

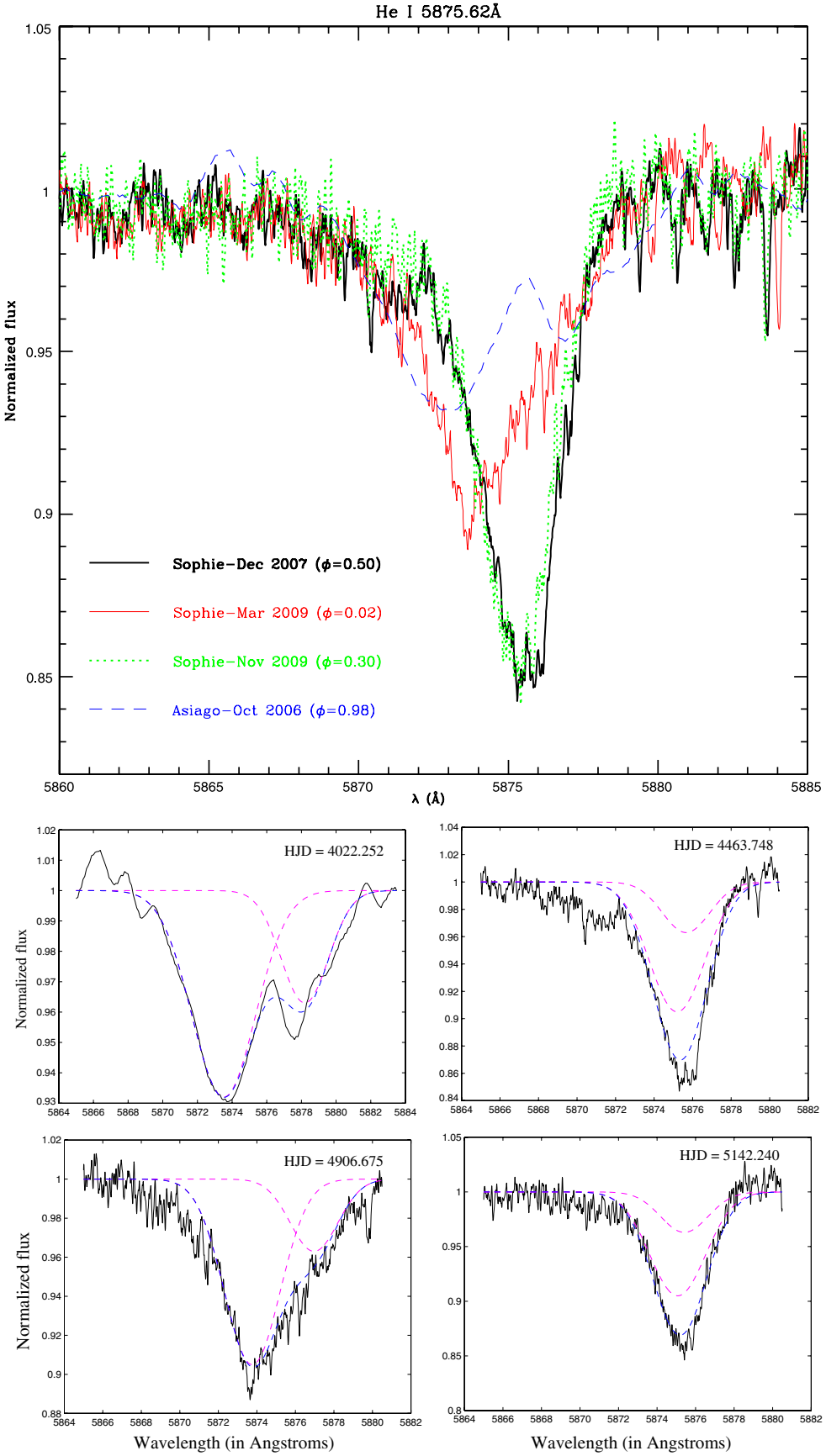

Figure 1. Top panel: He I λ5876 line in the Sophie data of HJD 4463.748 (thick solid black line), 4906.675 (thin solid red line, data taken half an orbit later than the previous ones), and 5142.240 (dotted thick green line, data taken a quarter of an orbit later than previous ones), as well as the Asiago data of the 2006 periastron passage (4022.252, dashed blue line). Quoted phases are from the SB2 solution (second column of Table 3). Middle and bottom panels: deblending using the χ^2 method for these spectra.

(A color version of this figure is available in the online journal.)

Table 3
Preliminary Orbital Solution for Cyg OB2 No. 9

Parameter	SB2	SB1 for Primary	SB1 for Secondary	SB1 for ($RV_1 - RV_2$)	SB1′ for ($RV_1 - RV_2$)	SB2′
P (d)	852.9 ± 4.3	858.6 ± 7.0	848.4 ± 3.0	851.4 ± 5.5	851.3 ± 5.6	852.8 ± 4.4
T_0	4036.8 ± 3.6	4019.3 ± 5.7	4047.6 ± 2.3	4036.5 ± 4.4	4031.0 ± 4.9	4030.9 ± 3.9
e	0.744 ± 0.030	0.752 ± 0.033	0.799 ± 0.033	0.736 ± 0.036	0.704 ± 0.034	0.708 ± 0.027
ω (°)	−164.4 ± 4.1	167.1 ± 5.8	33.5 ± 4.8	−166.5 ± 5.3	−176.4 ± 5.9	−175.1 ± 4.4
M_1/M_2	1.17 ± 0.22			1.27 ± 0.35	1.16 ± 0.26	1.10 ± 0.17
γ_1 (km s^{-1})	−40.6 ± 3.2	−38.5 ± 2.0		−38.9 ± 4.0	−24.4 ± 5.3	−28.1 ± 3.4
γ_2 (km s^{-1})	16.6 ± 3.5		18.9 ± 2.0	17.8 ± 4.0	2.2 ± 5.3	1.2 ± 3.5
K_1 (km s^{-1})	53.0 ± 7.0	59.6 ± 6.5		50.3 ± 11.0	62.3 ± 10.7	63.2 ± 6.8
K_2 (km s^{-1})	62.1 ± 8.1		73.2 ± 7.7	63.9 ± 11.0	72.0 ± 10.7	69.4 ± 7.4
$a_1 \sin i$ ($R_\odot$)	598.0 ± 84.4			572.9 ± 129.6	744.3 ± 132.7	752.1 ± 86.0
$a_2 \sin i$ ($R_\odot$)	699.3 ± 97.7			727.8 ± 132.2	860.2 ± 134.3	825.9 ± 93.7
$M_1 \sin^3 i$ ($M_\odot$)	21.7 ± 7.2			22.8 ± 10.2	41.0 ± 15.4	38.0 ± 10.1
$M_2 \sin^3 i$ ($M_\odot$)	18.6 ± 6.1			17.9 ± 8.7	35.5 ± 14.0	34.6 ± 9.1
rms (km s^{-1})	14.5	11.6	8.1	14.0	12.5	16.3

Note. SB1′ and SB2′ refer to the use of identical velocities when the lines are blended (see the text).

was derived from it using the best-fit result among the solutions calculated using methods by Wolfe et al. (1967) and Lehmann-Filhés (1894). The former method relies on the derivation of the Fourier expansion (limited to two terms) of the observed RV curve followed by an identification of the coefficients with those issued from a series expansion of the theoretical RV curve corresponding to a Kepler orbit; the latter method uses the amplitude and various integrations under well-defined parts of the RV curve to get a first estimate of the orbital parameters. From that starting point, a refined, final solution was found using a Levenberg–Marquardt minimization on a method adapted to eccentric binaries ($e > 0.03$) by Schlesinger (1910). A check of the correctness of the orbital solution was made based on the recent algorithm of Zechmeister & Kürster (2009) which, by performing the fit in terms of the true anomaly, reduces the nonlinearity of the RV curve to three free parameters instead of six (the other three free parameters then being readily derived from the periodogram coefficients); only a few iterations of the Levenberg–Marquardt method are then needed to reach the final solution, which, in our data sets, always agrees with the result of the first derivation. Errors were estimated using the diagonal of the variance–covariance matrix. The SB1 fitting was performed on the RVs of the primary, on the RVs of the secondary, and on the velocity difference between the primary and the secondary.

Double-lined spectroscopic binary (SB2) solutions relied on the main idea of the Liège Orbital Solution Package (LOSP).[7] In this method, the secondary and primary velocities are converted into an equivalent SB1 data set, using a linear orthogonal regression fit between the velocities of the two components. After this transformation, the equivalent SB1 data set was fitted as described above.

In both cases, the period was allowed to vary slightly, since van Loo et al. (2008) had a relatively large uncertainty ($P = 2.355 \pm 0.015$ yr) and our observations were taken 10–13 cycles after the radio data. Indeed, the phase of the 2006 October and 2009 February periastron passages seems to occur at $\phi = 0.95$ rather than at 0.0 (Figure 2). However, since we cover only two events of maximum separations, the formal improvement on the period error from our sole data set is not very large.

Table 3 gives the derived orbital parameters and their associated error bars, while Figure 3 graphically shows the results

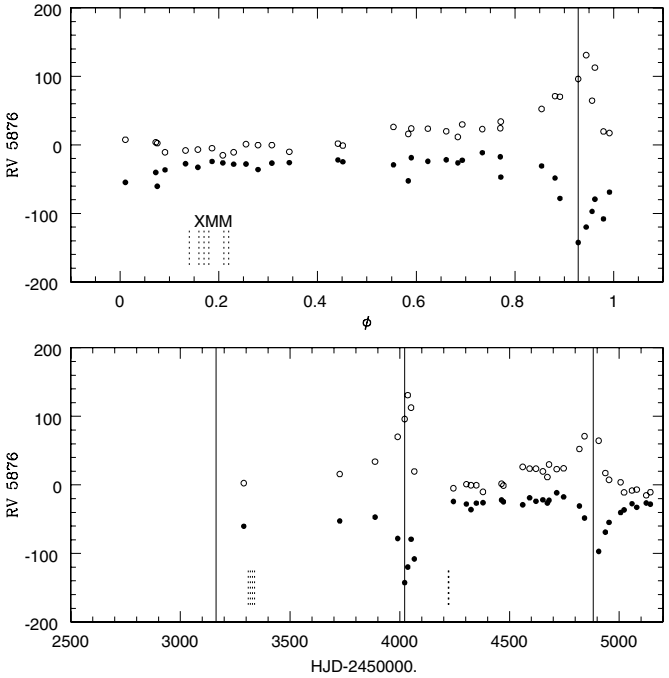

Figure 2. Evolution of the RVs of He I λ5876 measured by the χ^2 method with time (bottom panel) and phase (top panel, using the ephemeris from van Loo et al. 2008). The primary (resp. secondary) RVs are shown in filled (resp. open) circles; vertical lines indicate 2006 October 13 (HJD 4022.252), the approximate date of the periastron passage, and the dates 2.355 yr before/after. Dotted lines indicate the phases or dates at which the *XMM-Newton* data were taken.

of the best SB2 solutions. Note that smaller weights were given to the lower-quality data (0.3 for WIRO and 0.6 for Asiago and SPM, 1 otherwise).

The best orbital solutions rely on our best estimates of the RVs, i.e., those derived from the χ^2-mapping. In each case, the best-fit period is slightly revised downward but agrees well, within the errors, with the radio determination. As it takes into account both components, the SB1 solution calculated on the RV difference agrees best with the results of the SB2 solution, though the parameters derived for the individual SB1 solutions are never at 3σ from the results of the SB2 solution. The mass ratio is close to unity, confirming the similarity of the two stars of Cyg OB2 No. 9 found by Nazé et al. (2008) who proposed spectral types of O5+O6–7. Using the typical masses of such

[7] The LOSP package and a preprint describing it (Sana & Gosset 2010) can be downloaded from http://staff.science.uva.nl/~hsana/losp.html.

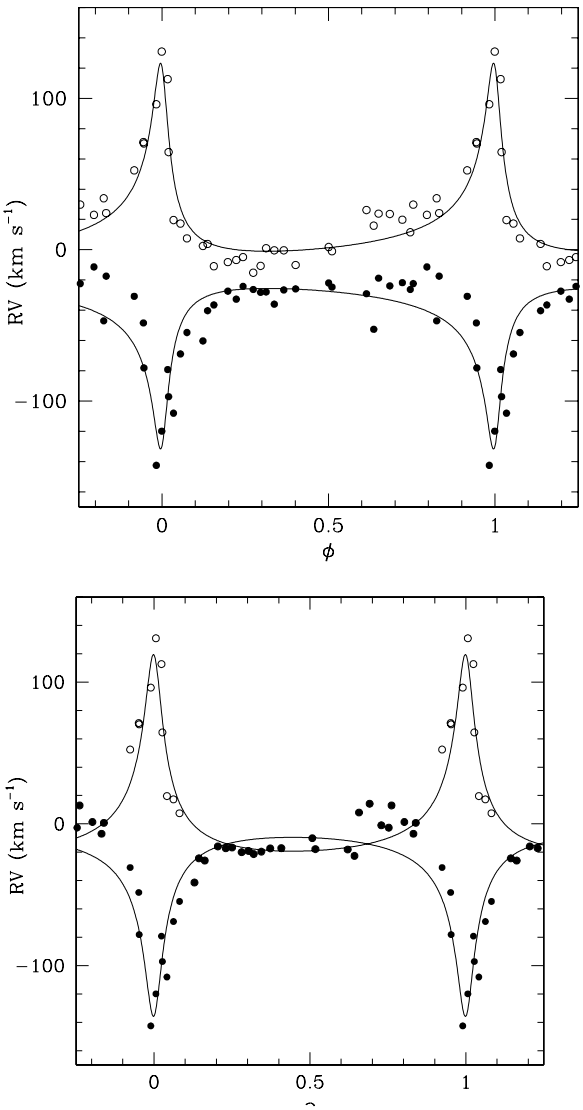

Figure 3. RV curves superimposed on the best SB2 solutions (SB2 shown on the top panel, SB2′ on the bottom panel). The symbols are as before and the errors on the velocities are on the order of 10–20 km s^{-1}.

stars as quoted in Martins et al. (2005), the masses derived from the χ^2-mapping imply an inclination of about 45°–50° if both components are supergiants, or 55°–60° if both components still belong to the main sequence (which is unlikely in view of the combined O5I spectral type). The eccentricity is large, as previously suspected, with a value of about 0.7–0.75. The velocities of the center of mass are quite different for both stars, as could be expected from the fact that the secondary lines are never seen on the blue side. Indeed, our RV curves do not cross (see Figure 3, left) but, as already mentioned, the RV determination when lines are totally blended is difficult and a slight crossing (by, e.g., 10 km s^{-1}) of the true RV curves therefore cannot be totally excluded. In any case, it would not change the fact that the center-of-mass velocity of the primary is blueshifted compared to that of the secondary. This is most probably related to the fact that the wind of the primary is stronger than that of the secondary, leading to the formation of the stellar lines of the most extreme star (the primary) not at the photosphere but farther in the wind itself.

As the RVs are uncertain when the lines are blended, i.e., for 80% of the orbit, we checked our results by calculating orbital solutions using the RVs from χ^2-mapping only when the lines are unblended, i.e., near periastron, and the results of a single Gaussian fit otherwise (i.e., for $0.1 < \phi < 0.9$). The weights were halved when the RVs of the primary and secondary are supposed identical. These solutions are given in the last columns of Table 3 and shown in Figure 3 (bottom panel); they are identified by a "prime" sign. As could be expected, the difference between the center-of-mass velocities is reduced and the semi-amplitudes are slightly enlarged. It must however be noted that the orbital parameters are similar, within the 1σ error bars (except for the center-of-mass velocities, which agree within 2σ). The largest differences are seen in the physical parameters, as the larger amplitudes naturally result in larger masses and semi-axes, hence suggesting larger inclinations (∼70° in the case of supergiants, ∼90° for main-sequence objects).

Table 4
Journal of the *XMM-Newton* Observations, with Heliocentric Julian Dates Given in the Format HJD-2,450,000 and Phases From the SB2 Solution (second Column of Table 3)

Obs	Date	ϕ	MOS1	MOS2	pn
1	3308.583	0.14	0.148 ± 0.004	0.162 ± 0.004	0.406 ± 0.007
2	3318.558	0.16	0.138 ± 0.004	0.151 ± 0.004	0.397 ± 0.008
3	3328.543	0.17	0.135 ± 0.004	0.141 ± 0.004	0.303 ± 0.005
4	3338.505	0.18	0.131 ± 0.004	0.143 ± 0.005	
5	4220.355	0.21	0.108 ± 0.004	0.100 ± 0.004	0.301 ± 0.007
6	4224.170	0.22	0.108 ± 0.004	0.109 ± 0.003	

Note. Xspec count rates (in counts s^{-1}) within the extraction region are given for the three instruments in the 0.4–10 keV energy band.

4. THE X-RAY EMISSION FROM Cyg OB2 No. 9

X-ray emission from Cyg OB2 was discovered serendipitously when *Einstein* was pointed at Cyg X-3 (Harnden et al. 1979). This was actually the first report of X-ray emission from OB stars. Since then, the region has been observed several times by X-ray observatories. The most recent exposures have been obtained thanks to a monitoring of Cyg OB2 No. 8a with *XMM-Newton* (see preliminary results in Rauw et al. 2005a).

4.1. The XMM-Newton Data set

In total, *XMM-Newton* provided six pointings centered on Cyg OB2 No. 8a (ObsId = 20045, 50511; PI: G. Rauw). The first four data sets, separated by 10 days each and with a duration of 20 ks, were obtained in 2004 October–November; the last two data sets, of length 30 ks, were taken three years later, around 2007 May 1 (Table 4). All exposures were obtained with the same EPIC configuration (full frame, medium filter). The reduction process of the first four data sets is explained in detail in De Becker et al. (2006). The last two were reduced in a similar manner and we only repeat here the most important information.

The raw data were processed with the SAS version 6.0 package. Some bad time intervals affected by high background events (so-called soft-proton flares) were rejected. A few stray-light features (due to singly reflected photons) from Cyg X-3 are visible in the lower right corner of the images. However, they do not affect the most interesting part of the field of view. The Cyg OB2 No. 9 data were extracted within a circle (of radius 40″ for the first four data sets, of radius 30″ for MOS, and 23.″25 for pn in the last two observations) centered on the source, whereas the background was extracted from a nearby 50″ × 20″ area devoid of X-ray sources. The EPIC spectra were

Table 5
Best-fit Parameter Models for Cyg OB2 No. 9 and X-ray Fluxes at Earth in the 0.5–10 keV Band

Obs	$\log N_{\rm wind}$ ($\rm cm^{-2}$)	kT_1 (keV)	$\rm Norm_1$ 10^{-3} ($\rm cm^{-5}$)	kT_2 (keV)	$\rm Norm_2$ 10^{-3} ($\rm cm^{-5}$)	χ^2_ν (dof)	$f_X^{\rm obs}$ (erg $\rm cm^{-2}$ $\rm s^{-1}$)	$f_X^{\rm corr}$ (erg $\rm cm^{-2}$ $\rm s^{-1}$)
1	$21.66^{+.09}_{-.10}$	$0.67^{+.12}_{-.04}$	$(3.41^{+0.83}_{-0.81})$	$2.39^{+.27}_{-.23}$	$(1.89^{+.28}_{-.18})$	0.86 (391)	1.66×10^{-12}	5.35×10^{-12}
2	$21.56^{+.11}_{-.15}$	$0.63^{+.05}_{-.04}$	$(2.58^{+0.70}_{-0.64})$	$2.21^{+.19}_{-.13}$	$(2.10^{+.16}_{-.18})$	0.89 (423)	1.60×10^{-12}	5.24×10^{-12}
3	$21.69^{+.06}_{-.05}$	$0.62^{+.03}_{-.03}$	$(4.21^{+0.68}_{-0.87})$	$2.40^{+.20}_{-.23}$	$(1.95^{+.25}_{-.17})$	1.16 (414)	1.74×10^{-12}	5.91×10^{-12}
4	$21.80^{+.12}_{-.13}$	$0.61^{+.07}_{-.12}$	$(4.49^{+3.07}_{-1.36})$	$2.69^{+.69}_{-.41}$	$(1.80^{+.34}_{-.37})$	0.95 (122)	1.69×10^{-12}	5.04×10^{-12}
5	$21.85^{+.07}_{-.08}$	$0.50^{+.11}_{-.05}$	$(5.45^{+1.88}_{-2.19})$	$2.43^{+.28}_{-.28}$	$(1.92^{+.18}_{-.22})$	0.94 (211)	1.52×10^{-12}	4.73×10^{-12}
6	$21.70^{+.10}_{-.14}$	$0.64^{+.08}_{-.05}$	$(3.10^{+1.01}_{-0.96})$	$2.44^{+.34}_{-.30}$	$(1.80^{+.27}_{-.24})$	0.79 (155)	1.53×10^{-12}	4.67×10^{-12}

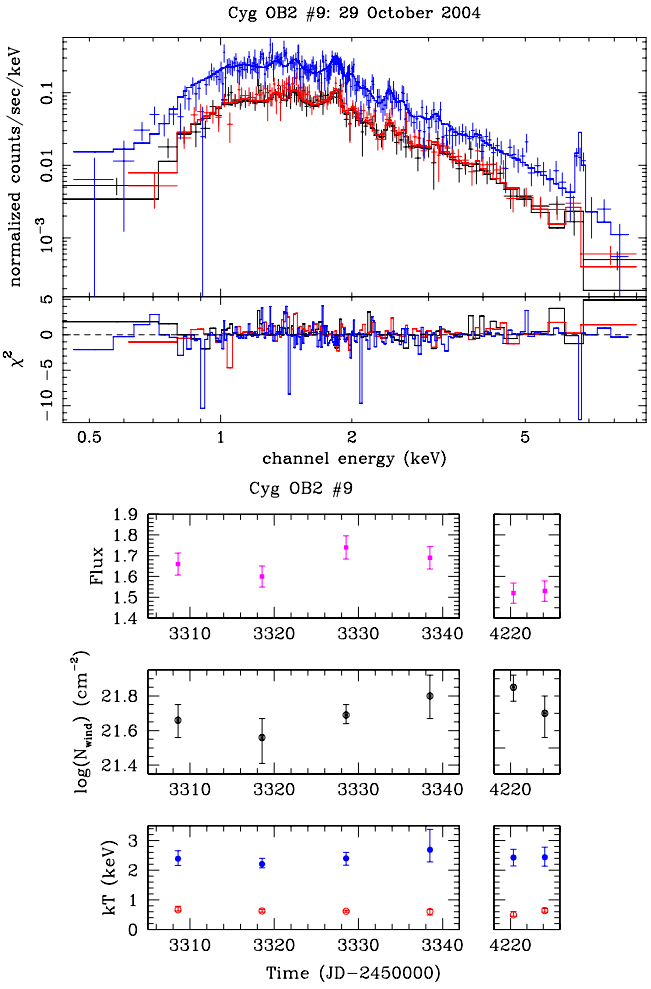

Figure 4. Top panel: EPIC spectra of Cyg OB2 No. 9 and the best-fit model in the first observation (lower lines: EPIC-MOS1 in black + MOS2 in red; upper line: pn in blue). Bottom panels: variations of the fitted parameters through the observations.

(A color version of this figure is available in the online journal.)

analyzed with the xspecv11.2 software. Note that the EPIC-pn data of Cyg OB2 No. 9 in Obs 4 and 6 are not available due to the source falling partially or totally in a CCD gap.

4.2. X-ray Properties

In the radio range, Cyg OB2 No. 9 displays a clear signature of non-thermal emission. Indeed, considering its quite long period, Cyg OB2 No. 9 fits in the so-called standard scheme for colliding-wind massive binaries accelerating particles, and producing synchrotron radiation in the radio domain (De Becker 2007). However, its X-ray emission, revealed by our *XMM-Newton* observations, appears clearly thermal in nature, as several X-ray lines are detected in the spectra (e.g., the iron line at 6.7 keV; see Figure 4). In fact, this strong thermal X-ray emission could easily hide, in the 1–10. keV range, a faint putative non-thermal X-ray component due to inverse Compton scattering. To be unveiled, such an X-ray emission should be investigated using observatories with a large sensitivity above 10 keV, where the thermal emission becomes negligible (De Becker et al. 2009).

To obtain a good fit to the observed *XMM-Newton* spectra, the combination of two hot, optically thin plasma was needed, and the fitted models are thus of the type $\rm wabs_{int} \times abs_{wind} \times (mekal_1 + mekal_2)$. The first absorption corresponds to the interstellar one, fixed to $N_{\rm H,ISM} = 1.15 \times 10^{22}$ $\rm cm^{-2}$. This value was derived from the reddening of Massey & Thompson (1991) and the gas-to-dust ratio of Bohlin et al. (1978). To allow for additional, circumstellar absorption, a second absorbing component was added and allowed to vary. As the circumstellar material is actually an ionized wind, we used the dedicated opacity tables from the wind absorption model of Nazé et al. (2004), as for Cygnus OB 8a in De Becker et al. (2006). Table 5 lists the best-fit models obtained for the six pointings. Note that $f_X^{\rm corr}$ corresponds to the dereddened flux, i.e., the flux corrected for the interstellar absorption.

The overall luminosity is rather typical of O stars. Using the bolometric correction of Martins et al. (2005) for an O5I star (the combined type of Cyg OB2 No. 9), as well as the V magnitude and reddening from Massey & Thompson (1991), the $\log(L_{\rm X}/L_{\rm BOL})$ is found to be −6.3, close to the typical value of this ratio for O-type stars (−6.45 with a dispersion of 0.51 dex in the 2XMM survey; Nazé 2009). The average temperature ($\langle kT \rangle = \sum(kT_i \times \rm norm_i)/\sum(norm_i)$) derived from the fits is 1.2 keV, which is slightly high compared to the average temperatures derived in the 2XMM (where 83% of the objects have $\langle kT \rangle$ below 1 keV). In fact, when accounting for the severe interstellar medium (ISM) absorption, the spectral shape appears similar to that derived in the 2XMM for HD 168112, another non-thermal radio emitter, at its lowest luminosity (Nazé 2009). Cyg OB2 No. 9 is thus only slightly harder and slightly more luminous than "normal" stars. However, it must be kept in mind that (1) with its long period, the Cyg OB2 No. 9 binary is wide, and therefore the winds are quite diluted before colliding; (2) the observations were taken rather far away from the periastron passage, at phases ϕ=0.14–0.22 (Figure 2). Additional observations during such an event are needed before one can totally exclude a significant contribution from wind–wind collision to the X-ray emission of Cyg OB2 No. 9.

Finally, it must be noted that Cyg OB2 No. 9 presents some variations between our observations. While the overall spectral

shape changes only slightly, the flux clearly decreased in the last two observations by about 10%, and there seems to be some shorter-term variations of lower amplitude between the first four observations. The origin of such variations is unknown. The reason for the long-term 10% change cannot be constrained before securing periastron observations, but it could simply be linked to a brightening associated with strong wind–wind collisions around periastron (cf. the cases of WR140 and η Car).

5. CONCLUSION

Cyg OB2 No. 9 is a rare case of non-thermal (radio) emission associated with O stars. Such emission is now thought to be associated with wind–wind collision in a binary, and we showed two years ago that Cyg OB2 No. 9 was indeed a multiple system. However, understanding non-thermal emission requires modeling the winds in detail, which in turn requests more than a "simple" binarity detection.

The continuous monitoring of Cyg OB2 No. 9 has led us to the derivation of a first orbital solution. The period is long, 2.4 yr, in agreement with the observed long-term radio modulation; the system eccentricity is large, i.e., 0.7–0.75, while the mass ratio approaches unity: Cyg OB2 No. 9 is thus also one of the few known long-period O+OB binaries and one of the few O+OB systems presenting a high eccentricity. It should be noted that the RV curve of Cyg OB2 No. 9 is peculiar, with only one unblended configuration (blueshifted primary–redshifted secondary) seen at periastron. Near apastron, the small RV difference between the two components is compatible with the large eccentricity and the orientation of the orbit, but the absence of RV crossing (or a limited one) requires in addition a large difference in the center-of-mass velocities for the two components.

An additional monitoring was performed at high energies, with the hope of finding a signature of a wind–wind collision (which should be the origin of the non-thermal radio emission). In the X-ray range, however, Cyg OB2 No. 9 displays neither large overluminosity nor any strong enhancement of its hard emission. There is thus, at least outside periastron, no clear, unquestionable signature of X-ray emission from the wind–wind collision. However, the flux varies, on both short and long timescales, with a 10% brightness decrease between 2004 and 2007. The cause of these variations needs to be investigated, notably by getting data closer to periastron.

The next periastron passage of Cyg OB2 No. 9 should occur in 2011 June–July, this time without any solar conjunction problem. It is the best time for finishing the study of this object by performing a multi-wavelength campaign (simultaneous radio, X-rays, and optical monitoring), which will finally open the possibility of modeling the rare high-energy phenomena occurring in this system.

We thank E. Gosset for his advice on orbital solutions and statistics. The Liège group also acknowledges financial support from the FRS/FNRS (Belgium), as well as through the Gaia-DPAC and XMM+INTEGRAL PRODEX contracts (Belspo), the "Action de Recherche Concertée" (CFWB-Académie Wallonie Europe), the Scientific Cooperation program 2005–2006 between Italy and the Belgian "Communauté Française" (project 05.02), the European Community's Seventh Framework Program (FP7/2007-2013) under grant agreement number RG226604 (OPTICON), and the "Crédit d'impulsion ULg No. I-06/13" (ULg). Their travels to OHP were supported by the "Communauté Française" (Belgium). Finally, P. Eenens thanks Conacyt for its support.

REFERENCES

Abbott, D. C., Bieging, J. H., & Churchwell, E. 1984, ApJ, 280, 671
Benaglia, P. 2010, in ASP Conf. Ser. 422, High Energy Phenomena in Massive Stars, ed. J. Marti, P. L. Luque-Escamilla, & J. A. Combi (San Francisco, CA: ASP), 111
Bohlin, R. C., Savage, B. D., & Drake, J. F. 1978, ApJ, 224, 132
De Becker, M. 2007, A&ARv, 14, 171
De Becker, M., Blomme, R., Micela, G., Pittard, J. M., Rauw, G., Romero, G. E., Sana, H., & Stevens, I. R. 2009, in AIP Conf. Ser. 1126, SIMBOL-X: Focusing on the Hard X-ray Universe, ed. J. Rodriguez & P. Ferrando (Melville, NY: AIP), 347
De Becker, M., Rauw, G., & Manfroid, J. 2004, A&A, 424, L39
De Becker, M., Rauw, G., Sana, H., Pollock, A. M. T., Pittard, J. M., Blomme, R., Stevens, I. R., & van Loo, S. 2006, MNRAS, 371, 1280
Donati, J.-F., Babel, J., Harries, T. J., Howarth, I. D., Petit, P., & Semel, M. 2002, MNRAS, 333, 55
González, J. F., & Levato, H. 2006, A&A, 448, 283
Gosset, E., Royer, P., Rauw, G., Manfroid, J., & Vreux, J.-M. 2001, MNRAS, 327, 435
Güdel, M., & Nazé, Y. 2009, A&ARv, 17, 309
Harnden, F. R., Jr., et al. 1979, ApJ, 234, L51
Heck, A., Manfroid, J., & Mersch, G. 1985, A&AS, 59, 63
Hubrig, S., Schöller, M., Schnerr, R. S., González, J. F., Ignace, R., & Henrichs, H. F. 2008, A&A, 490, 793
Kiminki, D. C., et al. 2007, ApJ, 664, 1120
Knödlseder, J. 2000, A&A, 360, 539
Lehmann-Filhés, R. 1894, Astron. Nachr., 136, 17
Mahy, L., Rauw, G., Martins, F., Nazé, Y., Gosset, E., De Becker, M., Sana, H., & Eenens, P. 2010, ApJ, 708, 1537
Martins, F., Schaerer, D., & Hillier, D. J. 2005, A&A, 436, 1049
Massey, P., & Thompson, A. B. 1991, AJ, 101, 1408
Nazé, Y. 2009, A&A, 506, 1055
Nazé, Y., De Becker, M., Rauw, G., & Barbieri, C. 2008, A&A, 483, 543
Nazé, Y., Rauw, G., Vreux, J.-M., & De Becker, M. 2004, A&A, 417, 667
Rauw, G., De Becker, M., & Linder, N. 2005a, in Massive Stars and High-Energy Emission in OB Associations, ed. G. Rauw, Y. Nazé, R. Blomme, & E. Gosset, 103
Rauw, G., Sana, H., Gosset, E., De Becker, M., Arias, J., Morrell, N., Eenens, P., & Stickland, D. 2005b, in Massive Stars and High-Energy Emission in OB Associations, ed. G. Rauw, Y. Nazé, R. Blomme, & E. Gosset, 85
Sana, H., & Gosset, E. 2010, A&A, submitted
Schlesinger, F. 1910, Publ. Allegheny Obs. Univ. Pittsburgh, 1, 33
Sota, A., Maíz-Apellániz, J., Walborn, N. R., & Shida, R. Y. 2008, Rev. Mex. Astron. Astrofis. Conf. Ser., 33, 56
Sundqvist, J. O., Puls, J., & Feldmeier, A. 2010, A&A, 510, A11
van der Hucht, K. A. 2006, A&A, 458, 453
van Loo, S., Blomme, R., Dougherty, S. M., & Runacres, M. C. 2008, A&A, 483, 585
van Loo, S., Runacres, M. C., & Blomme, R. 2005, A&A, 433, 313
Wolfe, R. H., Jr., Horak, H. G., & Storer, N. W. 1967, in Modern Astrophysics. A Memorial to Otto Struve, ed. M. Hack (New York: Gordon & Breach), 251
Zechmeister, M., & Kürster, M. 2009, A&A, 496, 577
Zucker, S., & Mazeh, T. 1994, ApJ, 420, 806